ORIGINAL PAPER

Dick T. Claeson · William P. Meurer

Fractional crystallization of hydrous basaltic "arc-type" magmas and the formation of amphibole-bearing gabbroic cumulates

Abstract The Rymmen and Eriksberg gabbros preserve the crystallization products of hydrous basaltic liquids, ranging from anorthosite and troctolite to highly fractionated oxide gabbro, diorite, and leucotonalite. The high initial water content of the liquids that filled the magma chambers (1.5–3 wt%) allowed amphibole to saturate as an interstitial mineral even in the earliest formed cumulates. The increasing water content of the system helped to produce a thick sequence of cumulates with anorthitic plagioclase ($An_{87–92}$). The growth of interstitial amphibole caused much more interstitial liquid to be incorporated into the cumulates than might be expected for dryer basaltic systems, producing a very imperfect fractional crystallization process. Comparisons of models of the trace-element evolution of the two intrusions reveal that the overall enrichments of some elements are adequately predicted by a perfect fractional crystallization model but all agree better with an imperfect fractional crystallization model. This reflects the change in the bulk distribution coefficients of the solid assemblage upon amphibole saturation, with the retention of elements compatible in amphibole in the crystal pile and the loss of elements incompatible in amphibole from it. These results stress the importance of understanding the physical, as well as the chemical

processes involved in fractional crystallization and in particular the role of postcumulus processes.

Introduction

Studies of mafic intrusions have been focused on relatively "dry" systems (e.g., Parsons 1987; Cawthorn 1996) and therefore the knowledge of how "wet" mafic magmas differentiate at depth is limited. The presence of a significant amount of H_2O in a basaltic liquid changes its physical properties (lower viscosity, lower density, lower liquidus/solidus) and phase relations (Burnham 1979; Anderson 1980). The lower density and viscosity of the liquid may promote convection in the magma chamber and help to facilitate compaction in the accumulating crystal mush. Higher H_2O contents will also stabilize amphibole earlier during the crystallization of a basaltic liquid, producing a pronounced difference in bulk distribution coefficients for the solid assemblages in wet versus dry basaltic liquids. Early fluid saturation, which will occur in hydrous basaltic systems, also creates a larger potential for exsolved fluids to modify the solid assemblage and the fractionation path of the overlying liquid (Meurer and Boudreau 1998a, 1998b).

The Rymmen and Eriksberg gabbros are remarkably similar bodies that are part of the Proterozoic Transscandinavian Igneous Belt (TIB) in southern Sweden (Gaál and Gorbatschev 1987; Fig. 1). They preserve cumulates crystallized from relatively primitive, hydrous, high-alumina tholeiites and provide excellent opportunities to understand differentiation where "wet" magmas are envisaged at depth (e.g., Sisson and Grove 1993a, 1993b; Bindeman and Bailey 1999; Müntener et al. 2001; Grove et al. 2002). Here we present the field relations, petrography, whole-rock compositions, and both major- (microprobe) and trace-element (laser IC-PMS) compositions of the minerals of both intrusions. This helps to constrain intensive parameters such as

D. T. Claeson (✉)
Department of Geology, Earth Sciences Centre,
Göteborg University, Box 460, 40530 Göteborg, Sweden
E-mail: dick@gvc.gu.se
Tel.: +46-31-7732800
Fax: +46-31-7732849

W. P. Meurer
Department of Geosciences,
University of Houston, Houston, TX 77204-5007, USA

temperature, pressure, oxygen fugacity, and the major-element composition and initial H_2O content of the parental liquids. Inversion modeling of the bulk-rock compositions is used to determine the trace-element evolution of the differentiating liquids and these trends are compared to models of perfect and imperfect fractional crystallization to understand the role of amphibole crystallization in the crystal pile, in a fractionating basaltic system.

Field relations

The Rymmen gabbro

The Rymmen gabbro is part of the Småland-Värmland section of the TIB, and lies within the Protogine Zone (e.g., Gorbatschev 1980; Larson et al. 1990), a N–S-trending shear zone south of Lake Vättern that Wahlgren et al. (1994) interpreted as the Sveconorwegian Frontal Deformation Zone (Fig. 1). The Rymmen gabbro is approximately circular in exposure and 4 km in diameter (Fig. 2). The area is flat, with the highest exposures measuring 20 m above lake Rymmen. Contacts with the foliated TIB-granitoids are not exposed, but back-veining into the gabbro and partial melting of the surrounding granite close to the contacts indicate that the Rymmen gabbro is intrusive into the granitoids, consistent with radiometric dating on zoned zircon in the partially melted host rock (Claeson 1999b).

Modal layering is defined by variations in plagioclase, resulting in rocks that range between olivine melagabbro, troctolite, and anorthosite. Layering is most obvious in olivine-bearing rocks and is absent in quartz- and biotite-bearing rocks. It strikes E–W and dips between 60 and 90° to the south (Fig. 2). Higher modal proportions of olivine in the northern part and of Fe-Ti oxides in the southern part suggest that the floor of the intrusion is exposed along the northern margin. This is consistent with the cryptic layering and the dip of modal layering, all indicating that the intrusion is tilted towards the south. Magnetic susceptibility of outcrops also defines the layering in the intrusion (Fig. 3), and overall it shows a strong, positive magnetic anomaly, as do several other mafic intrusions in this part of the TIB (Wikman 2000).

Crystallization proceeded from the margins inward but the bulk of the cumulates (approximately 3 km) accumulated on the floor of the intrusion. Fe-Ti oxide-rich rocks mark the sandwich horizon, the meeting of the upward and downward growing crystallization fronts. Deformation and subsequent hydrothermal alteration is restricted to a few discrete shear zones. Thin (< 20 cm) ultramafic veins occur within the olivine-bearing parts of the gabbro and some are corundum-bearing (Claeson 1999a).

The Eriksberg gabbro

The Eriksberg gabbro (Magnusson 1925; Vinnefors 1985; Lundegårdh 1987) is situated in the Småland-Värmland granitoid belt, east of the Protogine Zone and
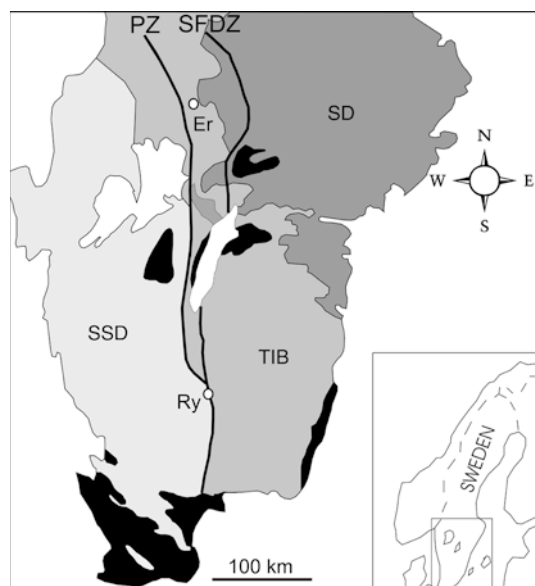
Fig. 1 Sketch map showing location of the Rymmen gabbro (*Ry*), the Eriksberg gabbro (*Er*) and tectonic subdivision of southern Sweden (modified after Juhlin et al. 2000). Key: 1, Svecofennian Domain (*SD*); 2, Transscandinavian Igneous Belt (*TIB*); 3, Southwest Scandinavian Domain (*SSD*); 4, Phanerozoic cover (*in black*). Protogine Zone (*PZ*), Sveconorwegian Frontal Deformation Zone (*SFDZ*)
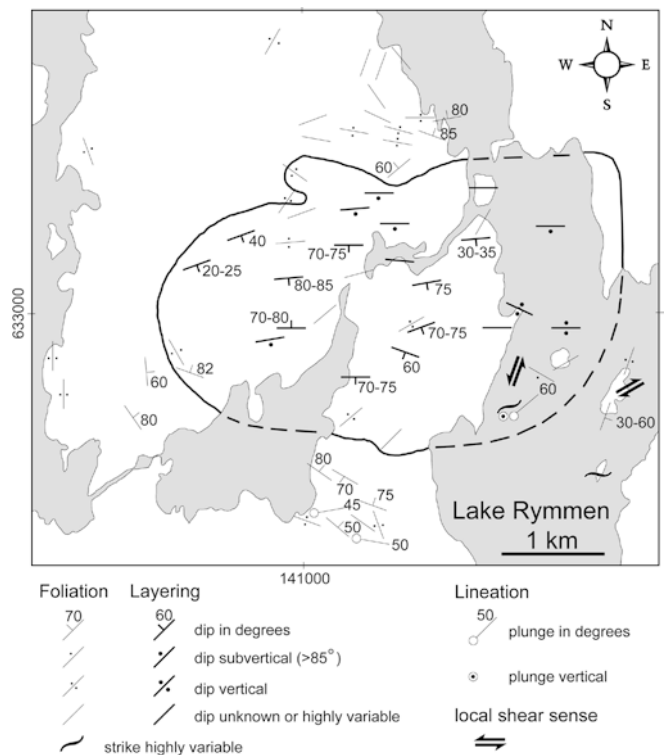
Fig. 2 Structure element map of the Rymmen gabbro, delineated by the *thin line*
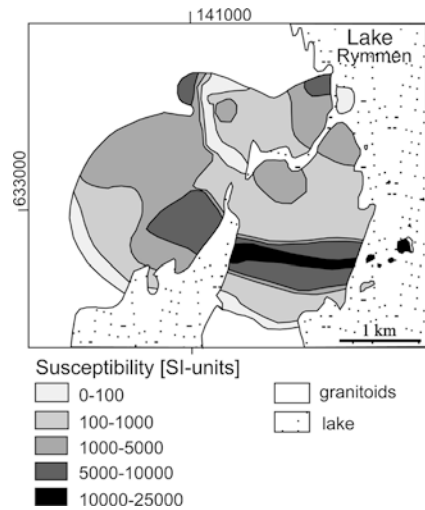
Fig. 3 Magnetic susceptibility map displaying the surface distribution of magnetic minerals within the Rymmen gabbro. Note that the susceptibility is high in the proposed roof section even where the whole-rock Mg# is relatively high (Fig. 5)

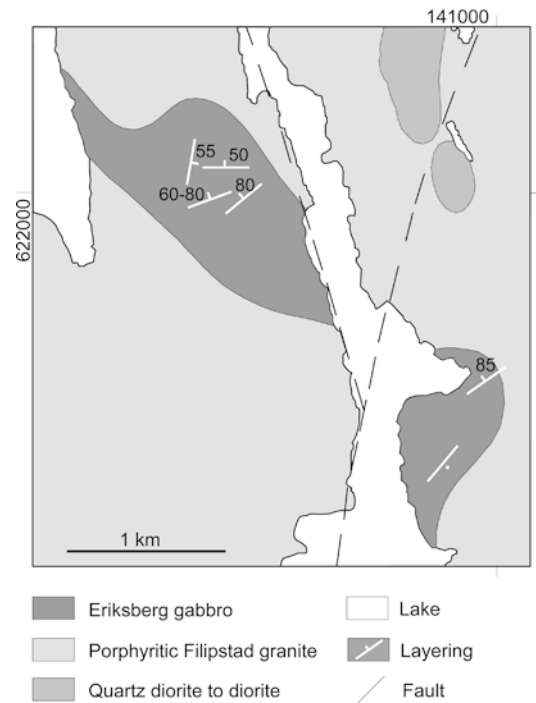Fig. 4 Sketch map of the Eriksberg gabbro with structure elements. Note that the quartz diorite to diorite on this map is not the rocks referred to in this study, which only accounts for rocks within the Eriksberg gabbro

west of the Sveconorwegian Frontal Deformation Zone (Fig. 1). The intrusion is deformed locally, but most of the igneous structures and textures are preserved. The gabbro shows clear intrusive relations with the host, forming apophyses within the granitoids that contain K-feldspar xenocrysts. There is less outcrop of the Eriksberg gabbro than of the Rymmen gabbro and much is hidden by lake Daglösen (e.g., a fault may cut the intrusion beneath the lake Fig. 4).

Both modal and rhythmic layering occur in primitive gabbros and the general features of the Eriksberg are similar to the Rymmen. However, a zone of diorite occurs in the southwest and leucotonalitic dykes, with pegmatitic contacts and fine-grained interiors, cut the gabbroic rocks of the Eriksberg gabbro. Leucotonalitic dykes are not found outside the intrusion indicating that they are local differentiates. Amphibole is present at some contacts between the gabbroic rock and the leucotonalitic dykes, and Vinnefors (1985) referred to the dykes as "gabbro pegmatite". Faults, locally filled with leucotonalite, are interpreted as synmagmatic and have displacements of 5 to 20 cm. These are most readily seen in rhythmically layered outcrops.

Mineral- and whole-rock compositions

Minerals were analyzed at the Earth Sciences Centre, Göteborg University, using a Zeiss® DSM 940 scanning electron microscope (SEM) with a Link® energy dispersive spectrometer (EDS) system for major-elements. We used an accelerating voltage of 25 kV, a sample current of about 1 nA, a counting live-time of 100 s, and calibrated with natural minerals and simple oxide standards. Cobalt was used as a reference standard and to minimize drift and the raw counts were reduced using a ZAF correction. Trace-element compositions were determined using a Cetac ASX-200 Nd-YAG UV laser for sampling and a HP-4500 quadrupole ICP-MS for analysis at Göteborg University. The procedures are detailed in Meurer and Claeson (2002) and estimated precision is approximately dependent upon elemental concentrations as follows: ≥10 ppm (better than 5%), 0.25–10 ppm (≤ 10%), 0.05–0.25 ppm (≤ 20%) and < 0.05 ppm (∼20–50%).

Petrography and major element characteristics

Rocks from the Rymmen and Eriksberg gabbros have many similarities and we summarize these common features first. The bulk of both intrusions are medium grained (1–5 mm) with rare plagioclase megacrysts (10–15 mm). Most samples are cumulates containing sub-euhedral cumulus grains surrounded by interstitial, postcumulus minerals. Early cumulates consist of cumulus plagioclase and olivine with interstitial magmatic hornblende, clinopyroxene, and orthopyroxene. These range from olivine melagabbro and olivine melagabbronorite, to troctolite (mela to leuco), and anorthosite. The evolved Fe-Ti oxide-rich gabbros and diorites contain plagioclase, ortho- and clinopyroxene.

Major-element mineral analyses from the main parts of each intrusion reveal a significant spread in compositions (Table 1). However, the major-element composition of cumulus plagioclase, present throughout both intrusions, is unzoned in early cumulates and mostly so
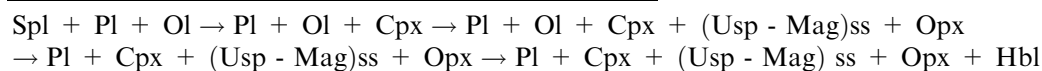
Table 1 Representative plagioclase, olivine, clinopyroxene, orthopyroxene and magmatic amphibole mineral analyses

Rock	Sample	Mineral	Na$_2$O	MgO	Al$_2$O$_3$	SiO$_2$	K$_2$O	CaO	TiO$_2$	Cr$_2$O$_3$	MnO	FeO	Sum
Hbl-dio	Ry95626	Plag	5.15		28.6	54.8	0.03	10.8				0.13	99.5
Gab-nor	Ry95084	Plag	3.70		30.8	51.9	0.02	13.5				n.d.	99.9
FeTi-ga	Ry95047	Plag	3.20		32.4	49.7	0.04	14.8				0.18	100.4
Gab	Ry95585	Plag	1.61		34.3	46.3	n.d.	17.6				0.11	99.9
Lol-gab	Ry95074	Plag	1.31		34.8	45.9	n.d.	18.2				n.d.	100.2
Ol-gab	Ry95597	Plag	1.23		34.7	46.1	0.01	18.4				n.d.	100.4
Ol-gab	Ry95605	Plag	1.03		35.7	45.5	0.04	18.7				0.07	101.0
Hbl-dio	Er96122	Plag	6.65		27.1	58.4	0.08	8.40				0.11	100.8
An-gab	Er96114	Plag	1.45		34.4	45.9	n.d.	17.8				0.25	99.8
Mel-gab	Er96119	Plag	1.25		34.5	45.6	0.01	17.9				0.20	99.4
Mel-gab	Er96100	Plag	1.10		35.6	45.5	0.04	18.3				n.d.	100.6
Gab	Ry95585	Oliv		38.8		38.5					0.33	23.0	100.7
Lol-gab	Ry95074	Oliv		40.9		39.2					0.30	20.7	101.1
Ol-gab	Ry95608	Oliv		41.8		39.1					0.27	19.2	100.4
Ol-gab	Ry95605	Oliv		42.6		38.7					0.29	19.1	100.7
An-gab	Er96110	Oliv		37.9		38.1					0.45	23.0	99.4
Mel-gab	Er96119	Oliv		39.4		38.6					0.34	22.2	100.5
Mel-gab	Er96100	Oliv		40.8		39.0					0.33	20.9	101.0
Gab-nor	Ry95084	Cpx	0.18	14.5	1.95	53.0		21.5	0.38	n.d.	0.43	8.69	100.6
FeTi-ga	Ry95047	Cpx	0.37	15.0	2.66	51.6		21.5	0.60	n.d.	0.26	7.77	99.8
Gab	Ry95585	Cpx	n.d.	16.2	2.89	53.0		21.8	0.43	0.36	0.17	6.36	101.1
Lol-gab	Ry95074	Cpx	n.d.	15.9	3.14	53.2		21.8	0.36	0.31	0.19	6.03	100.9
Ol-gab	Ry95597	Cpx	n.d.	16.0	3.18	52.2		22.9	0.44	0.42	0.11	4.27	99.6
Ol-gab	Ry95605	Cpx	n.d.	17.5	3.40	52.5		21.6	0.54	0.71	0.17	4.48	100.8
Hbl-dio	Er96122	Cpx	0.31	12.0	1.34	55.2		22.0	0.27	n.d.	0.54	10.9	99.7
An-gab	Er96110	Cpx	0.35	15.4	3.27	52.0		20.7	0.60	0.03	0.25	8.12	100.7
Mel-gab	Er96119	Cpx	0.28	16.1	1.38	53.6		23.1	0.26	0.20	0.22	5.36	100.5
Ol-gab	Er96106	Cpx	0.25	16.2	3.11	51.6		21.2	0.36	0.23	0.19	6.55	99.6
Gab-nor	Ry95084	Opx	n.d.	19.4	0.89	52.7		1.06	0.21	n.d.	1.10	25.7	101.1
FeTi-ga	Ry95047	Opx	0.17	23.3	1.66	52.7		1.31	0.29	n.d.	0.57	19.3	99.4
Gab	Ry95585	Opx	n.d.	28.5	1.59	54.7		0.98	0.18	0.12	0.38	13.3	99.7
Lol-gab	Ry95074	Opx	n.d.	29.1	1.70	55.4		0.64	n.d.	n.d.	0.41	13.4	100.7
Ol-gab	Ry95597	Opx	n.d.	29.8	1.84	54.9		0.84	n.d.	n.d.	0.30	12.2	99.8
Ol-gab	Ry95605	Opx	n.d.	29.7	1.62	54.6		0.91	n.d.	0.16	0.35	12.3	99.6
Mel-gab	Er96119	Opx	0.10	29.2	1.63	54.9		1.32	0.17	0.19	0.27	12.4	100.1
Mel-gab	Er96100	Opx	n.d.	29.7	1.11	56.1		1.09	n.d.	0.04	0.34	12.3	100.8
Hbl-dio	Ry95626	Amph	1.29	9.9	12.4	44.4	0.60	11.4	0.82	n.d.	0.37	16.8	97.9
Gab-nor	Ry95084	Amph	1.21	13.2	10.0	46.0	0.81	11.9	1.55	n.d.	0.22	13.1	98.1
FeTi-ga	Ry95047	Amph	2.05	13.5	13.3	43.9	0.70	12.0	1.83	n.d.	0.12	11.5	98.9
Gab	Ry95585	Amph	1.76	15.0	12.1	44.6	0.92	12.4	2.49	0.28	0.16	9.12	98.9
Lol-gab	Ry95074	Amph	2.06	17.4	12.4	45.6	0.24	12.5	0.43	n.d.	0.12	7.25	97.9
Ol-gab	Ry95597	Amph	1.95	17.3	13.2	45.9	0.33	12.4	0.83	n.d.	0.09	6.93	99.0
Ol-gab	Ry95605	Amph	2.01	16.6	16.7	43.2	0.16	12.1	0.09	0.10	0.12	7.08	98.1
Hbl-dio	Er96122	Amph	1.23	9.55	9.78	44.7	0.80	11.3	0.78	n.d.	0.45	18.6	97.2
An-gab	Er96114	Amph	1.55	15.4	11.5	45.4	0.79	12.3	0.70	0.38	0.10	9.79	97.9
Mel-gab	Er96119	Amph	2.75	16.6	12.9	43.5	0.26	11.4	0.80	0.33	0.17	8.63	97.2
Mel-gab	Er96100	Amph	2.04	16.8	11.6	44.8	0.44	11.4	2.70	0.04	0.11	8.25	98.2

n.d. not detected

in the evolved rocks. Inclusions of plagioclase are found in amphibole and clinopyroxene. Areas of symplectite that originally were inclusions of plagioclase are seen in olivine (Claeson 1998). Locally, coronas are developed where olivine is in contact with plagioclase (the mineralogy of the symplectites and coronas are discussed in the thermobarometry section below). The corona structures overprint interstitial amphibole and are interpreted as products of deuteric reactions (Claeson 1998). Clinopyroxene is unzoned, lacks exsolution features, and is both granular (cumulus) and interstitial, sometimes in the same sample with no detectable major element difference. Orthopyroxene is interstitial in olivine-bearing parts of the intrusions, but is cumulus in evolved parts. Amphibole is present in most samples, and in some thin-sections poikilitic amphibole is almost the only interstitial mineral. In early-formed cumulates, plagioclase and olivine reacted with the interstitial liquid to form amphibole (Meurer and Claeson 2002). Accessory pleonaste (green spinel), picotite, and chromian magnetite are present in early cumulates. The inferred order of crystallization is:

Spl + Pl + Ol → Pl + Ol + Cpx → Pl + Ol + Cpx + (Usp - Mag)ss + Opx
→ Pl + Cpx + (Usp - Mag)ss + Opx → Pl + Cpx + (Usp - Mag) ss + Opx + Hbl

The stages with ulvöspinel-magnetite solid solution are not well constrained for the Eriksberg gabbro (see below).

Features specific to the Rymmen gabbro

The outer parts of the Rymmen gabbro are the most primitive, followed by the central Fe-Ti oxide-rich samples, and the most evolved samples are at the same stratigraphic level as the central Fe-Ti oxide part but closer to the lateral margins (Fig. 5). Hornblende gabbro-diorite occurs as coarse-grained to pegmatitic rocks and is the most differentiated rock type found. Magnetite-ulvöspinel occurs in evolved cumulates and ilmenite is mostly found as exsolution lamellae in magnetite, and rarely as discrete grains coexisting with magnetite in the Fe-Ti oxide rocks.

Significant sidewall growth and lateral variations at the sandwich horizon make height above the floor an unreliable indicator of the evolution in the Rymmen gabbro. Therefore, we show the evolution of the system by ordering the samples based primarily on their position in the intrusion. For samples from near the sidewalls or roof we also use the anorthite content of plagioclase and molar $MgO/(MgO + FeO_T)$ of mafic silicates to construct an approximate stratigraphy (Fig. 6).

Features specific to the Eriksberg gabbro

Distinctive features of the Eriksberg gabbro include rare inclusions of clinopyroxene in olivine that have higher Mg# (88) and more calcic composition (CaMgFe = 48,

Fig. 5 Distribution maps showing An in plagioclase, Fo in olivine, Mg# in clinopyroxene, orthopyroxene, and amphibole, and whole-rock Mg#. The magnetic susceptibility contours from Fig. 3 are shown for comparison
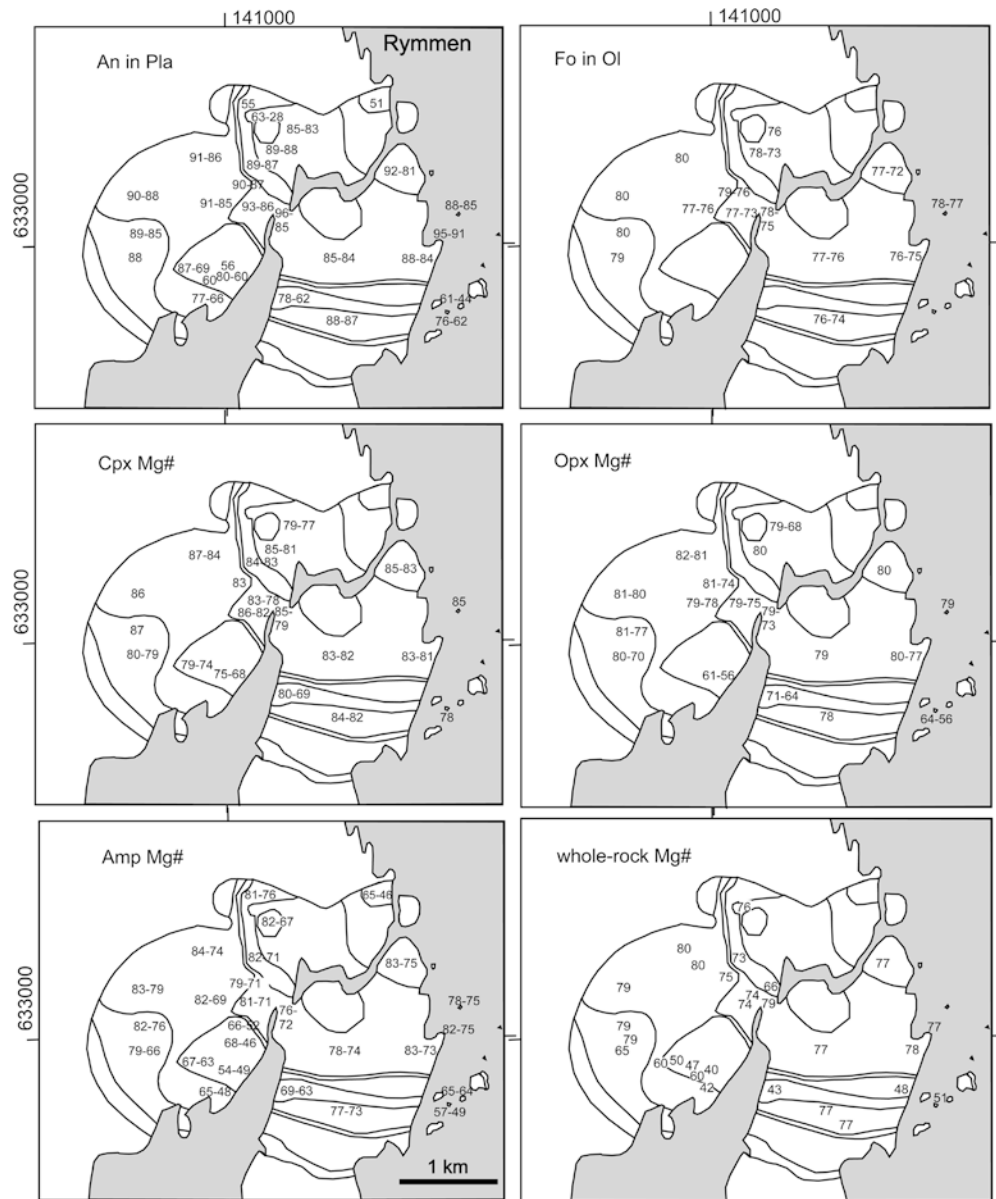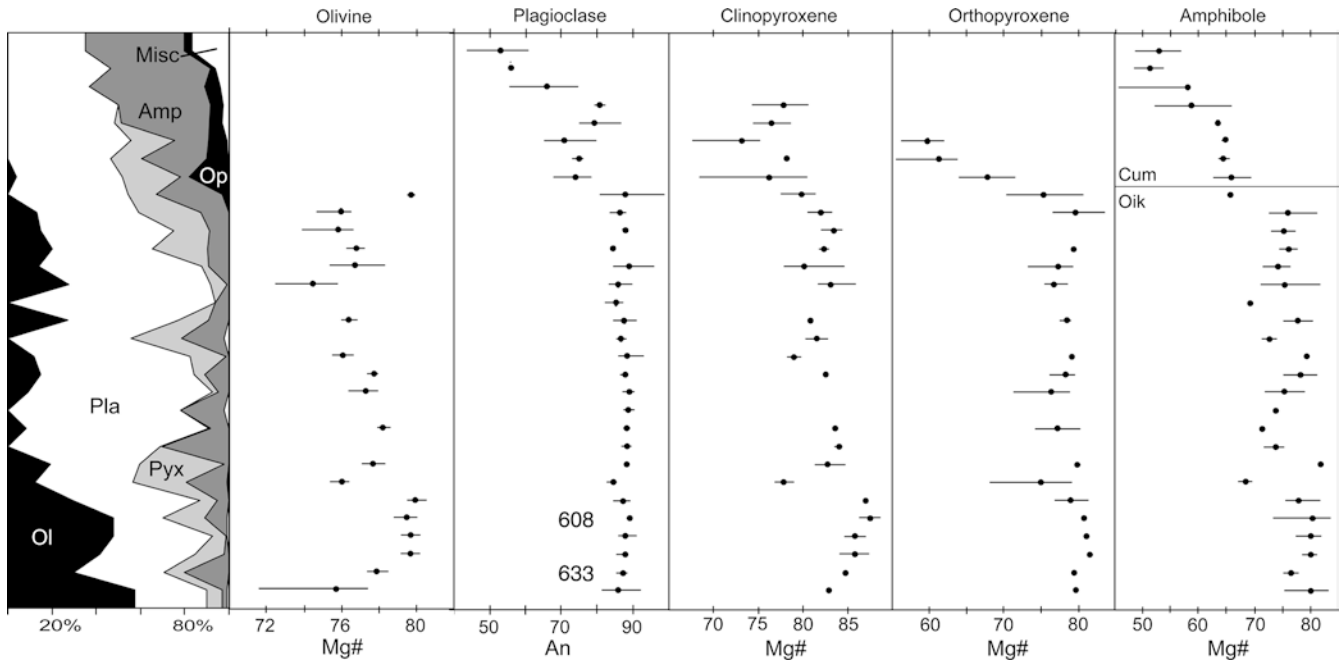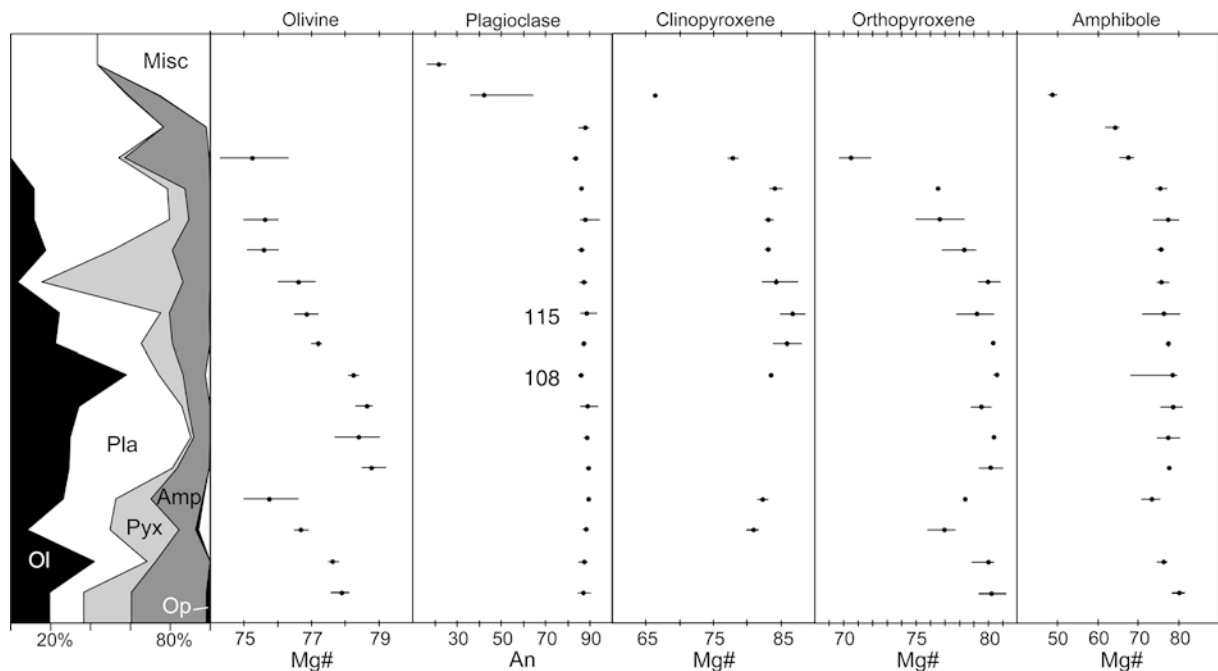
Fig. 6 Stratigraphic relations for the Rymmen gabbro, the first column shows the variation of the total mode ordered by the evolution of plagioclase and Mg/Fe silicates (see text). *Ol* olivine, *Pla* plagioclase, *Pyx* clino- and orthopyroxene, *Amp* amphibole, *Op* opaque minerals, and *Misc* biotite, quartz, k-feldspar, and other accessory minerals. The consecutive columns show variations in mineral compositions, where the *dot* marks the average and the *line* indicates the range. Samples 608 and 633, used for laser work, are marked in the plagioclase column

Fig. 7 Stratigraphic relations for the Eriksberg gabbro, ordered by the evolution of plagioclase and Mg/Fe silicates (see text and Fig. 5). Samples 108 and 115, used for laser work, are marked in the plagioclase column

46, 6) than other clinopyroxene. Gedrite, a Na-rich orthoamphibole typically restricted to metamorphic rocks, is an igneous mineral in an early-formed troctolitic cumulate (Claeson and Meurer 2002). Quartz and K-feldspar occur at the margins where partial melts of the surrounding granitoid have modified the liquid composition.

Extreme differentiates of the Eriksberg gabbro include diorite and leucotonalite dykes (Fig. 7). The hornblende diorite contains evolved plagioclase (An 36–42), rare clinopyroxene, and small remnants of cumulus orthopyroxene. The leucotonalite dykes contain quartz, plagioclase (An 10–25), K-feldspar, and

biotite as major minerals. Accessory minerals include apatite, zircon, monazite, allanite, Th-silicate (thorite or huttonite), and xenotime (Claeson 2002).

Mineral trace-element characteristics

Three primitive troctolites with interstitial clinopyroxene, orthopyroxene, amphibole, and biotite were selected for laser ablation ICPMS, two from the Rymmen gabbro and one from the Eriksberg gabbro. Analyses of plagioclase, clinopyroxene, orthopyroxene, amphibole, and biotite were collected for a more complete characterization of the intrusions and to use in comparison with the models of fractional crystallization discussed below. Analyses of clinopyroxene, amphibole, and biotite were collected using a 100 μm spot size and orthopyroxene and plagioclase using a 200 μm spot size (eTables 1, 2, 3, 4). For the cumulus minerals, we attempted to analyze core compositions but the spot size and potential complications of sampling a 3D object from a random 2D section means that some analyses may include evolved overgrowths. For the interstitial minerals, we analyzed the centers of large areas of these grains that are most likely to preserve the more primitive parts of these crystals (Meurer and Claeson 2002). The trace-element characteristics of the plagioclase and pyroxenes have compositions similar to these minerals crystallized from other basaltic liquids.

Plagioclase analyses from all samples show similar features. All show a significant range in incompatible element concentrations. For example, the La concentrations vary by a minimum of 6.5 times for sample 633 from the Rymmen gabbro to 10.5 times for sample 108 from the Eriksberg gabbro (eTable 1). We consider these minimum variations since we attempted to only analyze core compositions and so would suspect that analyses of rims might have resulted in an even larger observed variation. The incompatible element concentrations within each sample are correlated such that Y, Zr, the REE, Ba, Pb, Th, and U all define positive trends when plotted against one another. The coherent behavior of trace elements with a variety of geochemical characteristics strongly suggests that the variability reflects fractional crystallization and is not an artifact of inclusions or alteration in the analyzed grains.

Clinopyroxene and orthopyroxene trace-element compositions also show the compositional features associated with fractional crystallization (eTables 2 and 3). In the pyroxenes the variations are smaller, on the order of six times, than in plagioclase for most incompatible elements. Notable exceptions are Ba and Rb in both pyroxenes, which show large variations not correlated with other similarly incompatible elements (e.g., Th, U). Given the relatively mobile character of these elements it is likely that the high concentrations reflect small amounts of altered material included in the laser analyses. However, other variability in the pyroxenes clearly reflects the effects of fractional crystallization.

For example, orthopyroxene analysis 608–6 from the Rymmen gabbro has high Zr but low concentrations of REE and Sc, Ti, and V (eTable 3). These characteristics are consistent with growth of the orthopyroxene after a significant amount of amphibole crystallized and depleted the liquid in the Sc, Ti, V, and the REE but not in Zr (Meurer and Claeson 2002). Some of the orthopyroxene grains analyzed have particularly high concentrations of Co and especially Ni and likely formed by reaction of olivine with the liquid (e.g., 633–1 and 108–6). However, the majority of the orthopyroxene analyses and all of the clinopyroxene analyses have very limited ranges in their Co and Ni concentrations (eTables 2 and 3). The limited range in Co and Ni is consistent with the high and mostly invariant Mg# of these pyroxenes and suggests that the liquid composition was buffered by reaction with olivine.

Amphibole trace-element concentrations are highly variable both in regards to compatible elements (e.g., V, Ti) and incompatible elements (eTable 4), consistent with systematic changes during progressive crystallization reported in a detailed study of an amphibole from the Eriksberg gabbro (Meurer and Claeson 2002). For example, primitive amphibole REE patterns are similar in shape to those of clinopyroxene. With differentiation they become progressively depleted in the middle REE producing a flat negative slope and a slight positive Eu anomaly. The most evolved amphibole patterns are ''W''-shaped owing to the strong depletion of the middle REE except for Eu.

The Ti content in biotite is high in Eriksberg and low in Rymmen (eTable 4). However, Claeson and Meurer (2002) reported low Ti concentrations in biotite from another primitive cumulate from the Eriksberg, suggesting that the crystallization behavior of biotite is similar to that of amphibole. That is, both show large compositional variations in trace elements because they grew from an evolving interstitial liquid. The coupling of high Ti and low Zr in the biotite from the Rymmen, and low Ti and high Zr in the biotite from the Eriksberg, is similar to that seen in the detailed study of an amphibole oikocryst from the Eriksberg (Meurer and Claeson 2002).

Whole-rock chemical analysis

Whole-rock samples from the Rymmen (Table 2) and Eriksberg (Table 3) gabbros were analyzed by ICPMS and ICPAES at Activation Laboratories LTD, Ontario, Canada. Whole-rock analyses are of 5 to 6 kg samples that were percussion crushed, split, and then powdered in an agate swingmill. The international standard JB-1 was analyzed as an unknown and the observed and expected concentrations are given as a basis for assessing data quality (Table 2). The Pb concentrations in many of the samples are below the Act. Labs detection limit of 5 ppm. We therefore reanalyzed a primitive troctolite from the Rymmen gabbro by ICP-MS (at Göteborg

Table 2 Whole-rock major (wt%) and trace element (ppm) analyses of the Rymmen gabbro

Sample	95585	95596	95597	95607	95608	95623	96004	96005	96006	96007	96008	96009	96010	96011	95082	95605	95621	95626	94611	94612	JB-1	JB-1 lit.
SiO_2	46.44	46.11	42.21	41.58	39.47	44.68	45.09	45.01	43.29	41.96	45.28	45.88	39.80	43.98	46.39	40.74	41.92	50.27	51.90	47.20	51.11	52.37
TiO_2	0.19	0.87	0.06	0.08	0.11	0.10	0.08	0.11	0.08	1.59	0.18	0.12	0.14	1.44	1.28	0.10	0.05	1.05	0.13	0.70	1.28	1.32
Al_2O_3	17.42	17.38	21.50	15.73	12.57	28.20	27.64	24.54	21.17	17.13	17.49	19.84	11.46	17.08	18.01	15.42	20.57	15.58	18.70	17.20	13.90	14.53
Fe_2O_3	7.10	12.02	6.52	10.40	11.37	2.59	4.38	6.42	8.97	18.26	8.23	7.35	14.08	17.82	13.00	9.91	7.17	12.25	5.61	12.80	8.78	8.99
MnO	0.12	0.18	0.10	0.15	0.16	0.04	0.06	0.10	0.12	0.17	0.13	0.12	0.19	0.23	0.18	0.14	0.10	0.19	0.09	0.21	0.14	0.153
MgO	12.41	6.44	12.23	19.78	22.15	3.46	6.50	9.33	13.10	6.93	14.01	12.18	23.41	6.02	4.78	19.86	14.30	6.45	9.02	8.50	7.51	7.71
CaO	15.32	13.44	11.90	8.60	7.06	15.98	14.42	13.21	10.89	12.81	12.49	13.22	6.11	11.27	10.09	8.23	11.21	9.43	10.70	12.30	9.36	9.25
Na_2O	0.96	1.47	1.09	0.89	0.73	1.30	1.29	1.22	1.22	1.49	1.10	1.08	0.70	1.73	3.00	0.84	0.88	2.26	2.48	1.55	2.61	2.77
K_2O	0.10	0.33	0.07	0.11	0.13	0.43	0.15	0.19	0.10	0.22	0.16	0.17	0.10	0.35	0.53	0.12	0.06	0.70	1.02	0.39	1.34	1.43
P_2O_5	0.03	0.04	0.02	0.03	0.02	0.02	0.05	0.02	0.02	0.02	0.02	0.02	0.03	0.12	0.82	0.03	0.01	0.25	0.04	0.05	0.26	0.255
LOI	0.51	1.16	2.53	2.77	6.64	1.33	0.85	0.82	1.65	0.13	1.09	0.75	4.63	0.26	1.09	4.29	3.52	1.45	1.00	0.20	1.47	
Sum	100.63	99.77	98.27	100.17	100.58	98.13	100.52	100.97	100.60	100.70	100.17	100.72	100.65	100.28	99.16	99.68	99.79	99.89	100.69	101.10	99.09	
Mg#	77.6	51.5	78.8	79	79.4	72.6	74.6	74.2	74.3	42.9	77.1	76.6	76.7	40.1	42.1	79.9	79.8	51	76.1	56.8		
Sc	42	6	7	7	8	10	5	9	6	51	31	29	9	52	37	7	6	45	16.3	40	28	27.5
V	86	400	16	20	30	24	17	24	17	563	71	60	41	528	369	34	20	302	38.8	361	198	211
Co	53	53	66	100	115	17	36	49	75	71	75	59	118	57	37	95	70	40	41	57	37	38
Ni	99	5	88	257	251	18	36	74	121	n.d.	127	86	374	n.d.	n.d.	356	252	19	109	25.6	86	133
Pb	n.d.	n.d.	n.d.	n.d.	n.d.	n.d.	n.d.	n.d.	n.d.	n.d.	n.d.	n.d.	n.d.	n.d.	7	n.d.	n.d.	5	-	-	8	10*
Rb	2.3	12.3	1.7	2.8	13.1	20.6	4.0	4.8	1.5	4.7	2.8	3.7	1.9	10.8	22.5	2.9	1.1	22.0	58.1	13.2	38.7	41.3
Cs	0.2	1.3	0.2	0.9	2.7	1.4	0.5	0.5	0.2	0.3	0.3	0.53	0.35	0.94	2.1	0.3	0.1	1.3	-	-	1.37	1.23
Ba	89	170	93	103	72	87	107	110	86	115	90	98	70	171	240	76	59	217	142	151	537	493
Sr	297	371	370	191	221	474	454	398	398	372	303	321	212	352	525	302	392	348	304	378	390	444
Ta	0.03	0.06	0.01	0.02	0.01	0.01	0.01	0.01	0.01	0.02	0.01	0.01	n.d.	0.071	0.18	0.08	0.04	0.21	0.605	0.074	4.393	2.93
Nb	0.81	1.43	0.41	0.47	0.58	0.41	0.32	0.40	0.26	0.55	0.40	0.38	0.16	1.66	3.9	0.9	0.6	3.9	7.06	1.47	63.72	33.3
Hf	0.47	0.94	0.21	0.37	0.3	0.33	0.26	0.32	0.21	0.71	0.42	0.36	0.25	0.89	1.5	0.4	0.3	2.3	2.42	1.08	3.54	3.31
Zr	14.1	26.2	8.2	12.3	9.7	10.8	8.7	10.9	7.4	18.7	12.5	11.2	7.8	23.9	57	12	6.8	92	68	36.5	113	141
Y	6.2	12.4	1.7	2.2	2.4	2.7	2.2	2.9	1.8	10.1	5.3	4.6	2.4	17.6	27.8	2.6	1.3	22.4	12.4	13.5	23.7	24.3
Th	0.33	1.13	0.16	0.29	0.32	0.26	0.19	0.24	0.13	0.30	0.26	0.28	0.12	0.58	1.81	0.33	0.15	3.00	5.20	0.78	10.50	9.30
U	0.11	0.33	0.07	0.12	0.07	0.12	0.10	0.12	0.08	0.13	0.11	0.12	0.13	0.19	0.52	0.08	0.05	0.95	3.04	0.25	2.20	1.67
La	2.34	6.59	1.73	1.99	2.34	2.42	2.06	2.35	1.90	3.44	2.59	2.76	1.62	8.66	22.4	2.03	1.31	13.51	13	8.26	38.7	38.6
Ce	5.2	14.02	3.31	3.94	3.77	4.7	4.02	4.73	3.43	7.92	5.39	5.71	3.25	18.82	51.0	4.15	2.52	31.05	31.6	19.2	65.7	67.8
Pr	0.60	1.59	0.33	0.41	0.39	0.50	0.41	0.51	0.35	0.93	0.62	0.62	0.35	2.21	6.33	0.47	0.27	3.64	3.28	2.05	6.04	7.01
Nd	2.77	7.89	1.81	2.03	1.98	2.55	2.21	2.49	1.69	4.63	2.82	3.03	1.66	10.93	29.5	2.11	1.19	17.2	17.6	12.6	25.9	26.8
Sm	0.94	1.95	0.32	0.38	0.44	0.45	0.42	0.52	0.36	1.52	0.9	0.73	0.39	2.83	6.44	0.48	0.27	4.22	2.88	3.05	5.09	5.13
Eu	0.38	0.73	0.25	0.22	0.20	0.31	0.31	0.31	0.28	0.66	0.39	0.32	0.21	1.02	1.72	0.21	0.19	1.13	0.27	0.68	1.48	1.49
Gd	1.00	2.14	0.35	0.42	0.43	0.49	0.40	0.53	0.32	1.71	0.90	0.73	0.43	3.04	5.64	0.44	0.25	4.02	1.74	2.13	4.86	4.9
Tb	0.18	0.36	0.05	0.07	0.07	0.08	0.07	0.09	0.06	0.31	0.16	0.14	0.07	0.52	0.86	0.07	0.03	0.64	0.28	0.33	0.77	0.82
Dy	1.07	2.08	0.28	0.35	0.43	0.45	0.35	0.48	0.28	1.77	0.90	0.77	0.38	2.94	5.06	0.4	0.17	4.03	1.67	1.64	3.98	4.14
Ho	0.22	0.46	0.06	0.08	0.09	0.09	0.07	0.1	0.06	0.38	0.2	0.17	0.08	0.65	1.03	0.09	0.04	0.82	0.35	0.39	0.82	0.79
Er	0.61	1.29	0.17	0.23	0.25	0.27	0.21	0.3	0.19	1.07	0.55	0.49	0.24	1.86	2.81	0.25	0.12	2.41	0.79	1.23	2.32	2.27
Tm	0.09	0.20	0.02	0.04	0.03	0.04	0.03	0.04	0.03	0.15	0.08	0.07	0.04	0.28	0.35	0.04	0.02	0.32	0.16	0.14	0.34	0.35
Yb	0.55	1.34	0.16	0.24	0.25	0.23	0.2	0.28	0.18	0.97	0.47	0.45	0.25	1.87	2.14	0.26	0.15	2.06	1.15	1.06	2.18	2.13
Lu	0.09	0.19	0.03	0.04	0.04	0.04	0.03	0.05	0.03	0.14	0.08	0.07	0.04	0.28	0.33	0.04	0.02	0.35	0.16	0.17	0.31	0.31

n.d. not detected, (–) not analyzed. *JB-1*, Japanese basalt standard, was sent and analyzed as unknown. *JB-lit.* recommended or preferable (with asterisks) values for **JB-1**: Imai et al. (1995)
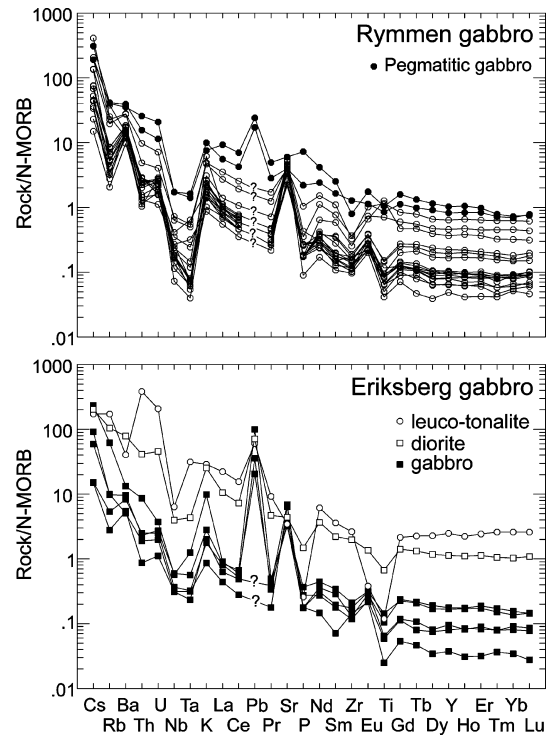
Table 3 Whole-rock major (wt%) and trace element (ppm) analyses of the Eriksberg gabbro

Sample	96100	96114	96115	96117	96118	96121	96122
SiO_2	41.13	43.50	41.57	45.41	75.89	45.34	54.04
TiO_2	0.17	0.03	0.07	0.13	0.15	0.08	0.83
Al_2O_3	12.25	26.67	18.01	12.82	13.16	28.30	17.36
Fe_2O_3	11.51	4.15	8.75	8.48	0.61	3.33	9.75
MnO	0.17	0.06	0.12	0.14	0.01	0.05	0.16
MgO	21.29	6.50	15.18	16.52	0.99	3.73	3.79
CaO	6.74	13.92	9.40	12.93	2.31	14.70	7.36
Na_2O	0.98	1.46	1.17	0.90	4.23	1.48	3.69
K_2O	0.19	0.06	0.12	0.14	2.07	0.69	1.79
P_2O_5	0.04	0.02	0.03	0.02	0.03	0.02	0.17
LOI	4.48	2.69	5.37	3.16	1.13	2.02	0.83
Sum	98.95	99.06	99.79	100.65	100.58	99.74	99.77
Mg#	78.6	75.6	77.5	79.4	76.3	68.9	43.5
Sc	13	3	7	43	3	7	24
V	65	17	33	110	11	35	198
Co	105	34	83	73	2	20	26
Ni	318	69	175	189	n.d.	47	12
Pb	28	n.d.	10	n.d.	18	6	21
Rb	5.1	1.5	2.8	5.4	96	34	57
Cs	0.6	n.d.	n.d.	0.4	1.2	1.6	1.4
Ba	57	33	49	31	254	82	486
Sr	270	554	360	299	307	602	388
Ta	0.07	0.04	0.04	0.03	4.13	0.16	0.56
Nb	1.3	0.7	0.8	0.7	14.7	1.3	9.1
Hf	0.5	0.4	0.3	0.4	2.7	0.4	3.2
Zr	14.6	10.2	8.1	9.2	193	12.6	144
Y	4.4	1	2.1	4.8	69.1	2.6	30.9
Th	0.26	0.1	0.28	0.22	45.8	1.01	4.87
U	0.12	0.05	0.11	0.09	9.74	0.17	2.1
La	1.97	1.05	1.89	1.52	55.1	2.19	25.9
Ce	4.68	2.01	3.69	3.54	116	4.38	53.8
Pr	0.61	0.23	0.42	0.49	12.10	0.51	6.08
Nd	3.03	1.03	1.87	2.54	44.4	2.22	26.23
Sm	0.84	0.18	0.44	0.73	9.39	0.5	5.7
Eu	0.30	0.21	0.22	0.28	0.39	0.31	1.36
Gd	0.78	0.19	0.39	0.84	7.85	0.42	5.08
Tb	0.13	0.03	0.05	0.14	1.5	0.07	0.87
Dy	0.72	0.15	0.32	0.84	10.29	0.36	5.25
Ho	0.16	0.03	0.08	0.17	2.24	0.08	1.09
Er	0.48	0.09	0.23	0.54	7.18	0.26	3.29
Tm	0.07	0.02	0.03	0.08	1.17	0.04	0.47
Yb	0.39	0.1	0.23	0.46	7.83	0.27	3.09
Lu	0.06	0.01	0.03	0.06	1.17	0.04	0.49

n.d. = not detected.

Fig. 8 Spidergram of whole-rock samples. The Pb detection limit is 5 ppm, data points below that are *question-marked*. N-MORB norm values from Sun and McDonough (1989). Note, only the top two samples in the Rymmen gabbro are from pegmatitic gabbros

Constraints on intensive parameters

Temperature, pressure, and oxygen fugacity

Mineral pairs with different parageneses provide information about magmatic and subsolidus mineral equilibration temperatures. The two-pyroxene geothermometers of Wood and Banno (1973), Wells (1977), and Powell (1978) give temperatures in the Rymmen gabbro from 930 to 1,065 °C (Claeson 1998) and in the Eriksberg gabbro from 920 to 1,005 °C. These are interpreted as reflecting the lower temperature range for crystallization. Primary amphibole-plagioclase geothermometery (Holland and Blundy 1994) in the Rymmen gabbro yields temperatures of 865 ± 35 °C at 6 to 8 kbar (Claeson 1998), the gabbroic rocks of the Eriksberg gabbro yield temperatures of 930 ± 65 °C at 4 to 6 kbar ($n = 22$), and in the Eriksberg diorite 741 ± 5 °C at 4 to 6 kbar ($n = 3$). The edenite-richterite thermometer was applied in all cases except where plagioclase was too calcic, X_{An} above 90. Temperature estimates for the formation of kelyphytic coronas in the Rymmen gabbro are 800 ± 30 °C at 6 to 8 kbar (Claeson 1998) and in the Eriksberg gabbro, using the amphibole-plagioclase geothermometer, yield 845 ± 15 °C at 4 to 6 kbar ($n = 18$). The temperatures derived from the primary amphibole-plagioclase mineral pairs either reflect the lowest magmatic temperatures or highest subsolidus temperatures. In contrast, the temperature

University) and determined a Pb concentration of 2.5 ppm, which agrees well with the concentration of Pb in the minerals. As the sample has low concentrations of other incompatible elements this value is considered a minimum and is used in the calculations below for samples with reported Pb < 5 ppm (See Fig. 8).

All samples show U and large ion lithophile element enrichments and Ti-Nb-Ta depletion relative to N-MORB (Fig. 4). All profiles are nearly parallel, except for those for the most evolved rocks, the pegmatitic gabbro of Rymmen gabbro and the leucotonalite in Eriksberg gabbro. The leucotonalite differs with higher Th, U, and Ta and lower Ti, Eu, and P. Two Fe-Ti oxide gabbros from the Rymmen gabbro with 9 and 17% opaques have positive Ti anomalies but all others have negative Ti anomalies, including a sample from the Eriksberg gabbro with 3% opaques.

from the coronas clearly reflects subsolidus mineral equilibration (Claeson 1998).

The kelyphytic coronas consist of enstatite ± amphibole and phlogopite, combined with an outer rim of symplectic intergrowth of green spinel and amphibole, and were used to deduce the emplacement depth of the Rymmen gabbro at 6 to 8 kbar (Claeson 1998). Kelyphytic coronas in the Eriksberg gabbro are neither as well developed nor as abundant as in Rymmen, which is an indication that the Eriksberg gabbro was emplaced at a shallower depth of 4 to 6 kbar. The magmatic amphibole geobarometers of Hammarstrom and Zen (1986) and Johnson and Rutherford (1989) agree with the pressure estimates based on the kelyphytic coronas (Claeson 2001).

Magnetite with exsolved ilmenite in the Rymmen and Eriksberg gabbros implies that most of the Fe-Ti oxide was originally magnetite-ulvöspinel solid solution. The almost total lack of primary ilmenite may be in part due to a low Ti content in the parental magmas (e.g., Frost et al. 1988; Vogel et al. 1999), but is primarily a consequence of differentiation at relatively high fO_2 (e.g., Snyder et al. 1993). According to the experimental results of Toplis and Carroll (1995) and Ariskin and Barmina (1999) magnetite-ulvöspinel is the first oxide to crystallize above the fayalite-magnetite-quartz (FMQ) buffer, and comparing the oxide mineralogy of the intrusions with the experimental data an estimate of FMQ + 1 or above is reached for both.

Constraints on initial magma compositions

The Mg#'s of the most magnesian mafic minerals of the Rymmen or Eriksberg gabbros are not in equilibrium with primary mantle melts. The equations of Roeder and Emslie (1970) and Wood and Blundy (1997) show that the Mg# of the equilibrium liquid for the most magnesian olivine or clinopyroxene is around 60 in both intrusions. This is below the proposed lower limit (64) for the Mg# of plagioclase-saturated liquids in equilibrium with the mantle (Longhi et al. 1999). The olivine and clinopyroxene compositions reflect either fractional crystallization of mantle derived liquids prior to emplacement, postcumulus re-equilibration, or both (e.g., Meurer and Boudreau 1998a, 1998b). The relatively low contents of Cr and Ni favor an earlier fractionation event.

With the notable exception of the interstitial amphibole, the Rymmen and Eriksberg magmas produced cumulates with assemblages typical of olivine tholeiites (e.g., Ghiorso and Carmichael 1985, 1987; Bartels et al. 1991) and so the magmas that filled the chambers are believed to have been hydrous, primitive tholeiites or picrites. The lack of K-feldspar in any uncontaminated rock of the Rymmen or Eriksberg gabbros, except for the leucotonalite, suggests an initially low K_2O magma (cf. Kushiro 1979). The low Na_2O in clinopyroxene, near the detection limit of the SEM-EDS, suggests low

magmatic Na_2O (Lundstrom et al. 1998). Salitic high-Ca clinopyroxene appears to result from a low silica activity in the liquid and is possibly an attribute of high H_2O activity (e.g., Beard and Borgia 1989; Gaetani et al. 1993; Shi 1993). The anorthite-rich composition of plagioclase in both intrusions, along with the presence of high-Al spinels, suggests a liquid composition low in Na and high in Al and H_2O (e.g., Beard and Borgia 1989; Sisson and Grove 1993a; Panjasawatwong et al. 1995; Pearce et al. 1995; Kuritani 1998; Bindeman and Bailey 1999).

Several lines of evidence indicate that the Rymmen and Eriksberg gabbros crystallized from a relatively hydrous liquid and on the basis of the following observations, we estimate the liquids that filled the chambers had between 1.5 and 3 wt.% H_2O. The high anorthite content in plagioclase, high wollastonite content in clinopyroxene, and magmatic hornblende indicate a hydrous magma (e.g., Gaetani et al. 1993; Sisson and Grove 1993a), as does the crystallization of primary orthopyroxene without any pigeonite (Cawthorn 1994). Interstitial amphibole occurs throughout both intrusions and is by far the most abundant interstitial mineral in some of the most primitive gabbros (Figs. 6, 7). If H_2O is the limiting component needed to initiate amphibole crystallization, this implies that the original H_2O content was less than but close to the ~2–3 wt% needed to stabilize amphibole. Estimates of less than 2–3 wt% H_2O (e.g., Tatsumi and Eggins 1995; Morra et al. 1997) are suggested for high-MgO arc basalts, whereas the H_2O content of hydrous high-alumina basalts is estimated at 3–6 wt% (e.g., Beard and Lofgren 1992; Kinzler et al. 2000). The bulk compositions of the intrusions suggest an initial liquid composition intermediate between these so we take 3 wt% H_2O as an upper limit for the initial water content.

Discussion

Interstitial amphibole and trace-element evolution

Most studies of fractional crystallization are based on cumulates formed by crystallization of relatively dry basaltic systems (e.g., the Bushveld and Stillwater complexes). Both theoretical (Shirley 1986; Meurer and Boudreau 1996), and observational (Meurer and Boudreau 1998a, 1998b) studies suggest that compaction of a crystal mush formed at the floor of these intrusions can result in near perfect fractional crystallization. Compaction has also been shown to be important in shallow sills (Shirley 1987) and even in thick basaltic flows (Philpotts et al. 1996). Comparison of the physical parameters of the dry and wet basaltic systems would seem to favor more efficient compaction with higher water contents. Additional water decreases the viscosity of the liquid and increases the density contrast between the solid and liquid, both of which favor faster compaction. In addition, the deep-seated emplacement of the

Rymmen and Eriksberg gabbros favors slow cooling, which should allow compaction more time to operate. However, textural and compositional analysis of cumulates from throughout both the Rymmen and Eriksberg gabbros indicate that significant postcumulus crystallization took place. In particular we find that, although not a cumulus mineral until late in the crystallization of these intrusions, amphibole is found in considerable amounts even in the most primitive cumulates (Figs. 6, 7).

Calculating the trace-element evolution of liquids from cumulate compositions

We evaluate the trace-element evolution of both intrusions and then compare these results to models of perfect (i.e., complete removal of interstitial liquid) and imperfect fractional crystallization (resulting in interstitial amphibole crystallization) to better understand the importance of early amphibole crystallization. The trace-element compositions of the parental and evolving liquids in both intrusions are estimated using a bulk-rock inversion. This model assumes that minerals interstitial to the cumulus grains precipitated from an equilibrium liquid and is based on the approach of Bédard (1994). The bulk distribution coefficient (D) of an element (i) is used to calculate the concentration of that element in the equilibrium liquid. The bulk D for element i, in minerals and liquid (j), is calculated according to Eq. (1), where α is the modal proportion and Kd is the Nernst distribution coefficient.

$$\sum_{j=1}^{n} \alpha^j Kd_i^j = D_i^{\text{Bulk}} \tag{1}$$

Kd-values used in the calculations are tabulated in Table 4. The crystallized liquid phase (CL) is assigned Kd = 1 (cf. Bédard 1994) and one minus the modal amount of cumulus minerals gives the modal proportion of CL. An example is given for Cs in an olivine gabbro in Eq. (2).

$$D_{Cs}^{\text{Bulk}} = \alpha^{ol} Kd_{Cs}^{ol} + \alpha^{cpx} Kd_{Cs}^{cpx} + \alpha^{pla} Kd_{Cs}^{pla} + \alpha^{CL} Kd_{Cs}^{CL} \tag{2}$$

Equation (3) is used to estimate the concentration of the element in the coexisting liquid by dividing the whole-rock concentration (WR^i) by the bulk D.

$$[Liq]^i = \frac{WR^i}{D_i^{\text{Bulk}}} \tag{3}$$

The critical assumptions in this model are that the interstitial minerals crystallized from a liquid initially in equilibrium with the cumulus minerals, and that the solid phases that grew from the interstitial liquid can be distinguished. This distinction is straightforward for minerals that are clearly not cumulus, such as accessory

Table 4 Kd values used in calculations

	ol	pla	cpx	opx	amp	mag
Cs	0.00015	0.015	0.001	0.00015	0.05	0.001
Rb	0.0002	0.015	0.001	0.0002	0.11	0.001
Ba	0.0003	0.4586	0.001	0.0005	0.43	0.001
Th	0.0003	0.05	0.0021	0.0007	0.41	0.02
U	0.0003	0.05	0.0028	0.0009	0.5	0.02
Nb	0.001	0.03	0.008	0.0013	0.76	0.04
Ta	0.001	0.03	0.013	0.0025	0.76	0.04
K	0.0002	0.097	0.001	0.0002	0.22	0.001
La	0.0003	0.124	0.0536	0.0008	0.2	0.015
Ce	0.0003	0.117	0.0858	0.0016	0.43	0.016
Pb	0.0003	0.13	0.0102	0.0121	0.2	0.0217
Pr	0.0003	0.105	0.124	0.0032	0.65	0.018
Sr	0.00036	1.83	0.1283	0.0012	0.49	0.022
P	0.0002	0.075	0.13	0.003	0.25	0.024
Nd	0.0002	0.068	0.1873	0.0056	1.23	0.026
Sm	0.00018	0.058	0.291	0.015	2.03	0.024
Zr	0.001	0.04	0.26	0.032	0.83	0.12
Hf	0.0029	0.04	0.33	0.06	0.83	0.97
Eu	0.0002	0.22	0.3288	0.03	1.73	0.025
Ti	0.002	0.043	0.34	0.086	3	20
Gd	0.00025	0.035	0.367	0.034	2.51	0.018
Tb	0.000475	0.031	0.404	0.054	2.7	0.019
Dy	0.0007	0.026	0.38	0.077	3.01	0.018
Y	0.001	0.026	0.412	0.095	2.58	0.018
Ho	0.00122	0.018	0.4145	0.1	2.9	0.018
Er	0.00174	0.0145	0.387	0.12	2.9	0.018
Tm	0.00348	0.012	0.4085	0.16	2.93	0.018
Yb	0.00522	0.0097	0.43	0.22	2.96	0.018
Lu	0.00852	0.008	0.433	0.22	2.59	0.018

Sources: Beattie 1993; Bédard 1994, 2001; Blundy 1997; Blundy and Shimizu 1991; Canil and Fedortchouk 2001; Chazot et al. 1996; Dunn 1987; Dunn and Sen 1994; Kennedy et al. 1993; Kohn and Schofield 1994; Meurer and Claeson 2002; Nielsen et al. 1992; Philpotts and Schnetzler 1970; Rollinson 1993; Watson et al. 1987

phases (e.g., apatite, zircon, sphene, etc.) in primitive cumulates. The incompatible element contribution of these minerals to the bulk rock composition is implicitly accounted for in the liquid component used in the calculation. Distinguishing other postcumulus growth is simplified by the oikocrystic habit of the pyroxenes and amphibole and by the fact that continued growth of plagioclase and olivine is halted when these minerals react with the liquid to form amphibole.

The quality of the bulk-rock inversions can be evaluated by comparing the calculated composition of minerals in equilibrium with the liquids and the observed mineral compositions in the rocks. Average laser ICPMS data from the cores of the minerals from two samples from each intrusion were used for the comparison. For most elements, the observed trace-element concentrations define a parallel trend that is displaced to slightly higher values than the calculated concentrations (Fig. 9). This is consistent with some re-equilibration of the mineral cores with evolved overgrowths on the rims and/or analyses that include rim material (we did not filter the data prior to averaging) and points out a potential pitfall to simply inverting the mineral compositions. The only trace elements that fall significantly off the trend are Th and U in clinopyroxene (observed > calculated) and Zr in plagioclase (observed < calcu-

Fig. 9 Comparison of calculated compositions of minerals in equilibrium with the bulk-rock inversion liquids and the observed mineral compositions in the rocks. Samples 608 (*filled*) and 633 (*unfilled*) (Rymmen) and 96108 (*filled*) and 96115 (*unfilled*) (Eriksberg). See text for discussion
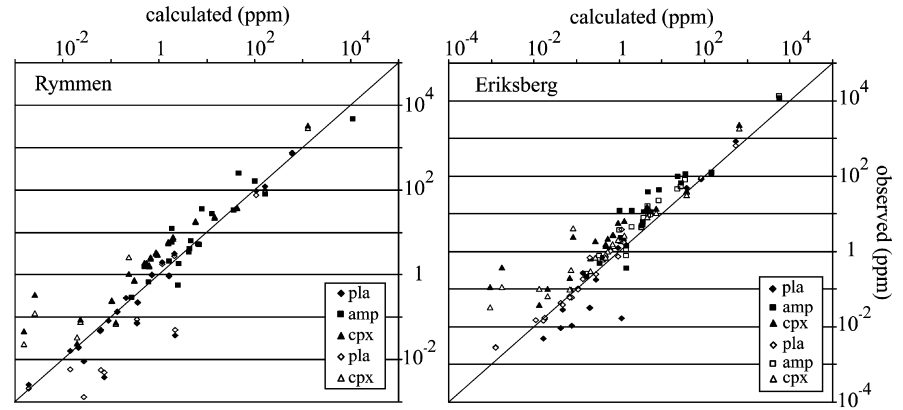

lated). The Kd's for Th and U in clinopyroxene used in these calculations are very low (0.001), and if correct, then a combination of kinetic effects and inclusion of evolved material in the analyses might explain the discrepancy. In three of four samples the Zr concentration in the plagioclase is much lower than expected suggesting that the Kd used for Zr in plagioclase is too high. Overall, the co-linear comparison suggests the bulk-rock inversion technique approximates the equilibrium liquid compositions.

Estimates of the percentage of the intrusion crystallized for each of the calculated liquid compositions were made so that the evolution of the systems can be evaluated. The percentage crystallized for the Rymmen gabbro was estimated based on the distribution of rocks in the intrusion. Limited outcrops make similar estimates for the Eriksberg gabbro difficult so we used a combination of sample distribution and composition, and analogy with the estimates for the Rymmen gabbro. Calculated liquids from rocks formed with less than

Fig. 10 N-MORB normalized spidergrams showing (**a**) trace-element inversions with estimates of fraction crystallized and model results for perfect (**b**) and imperfect (**c**) fractional crystallization for the Rymmen gabbro
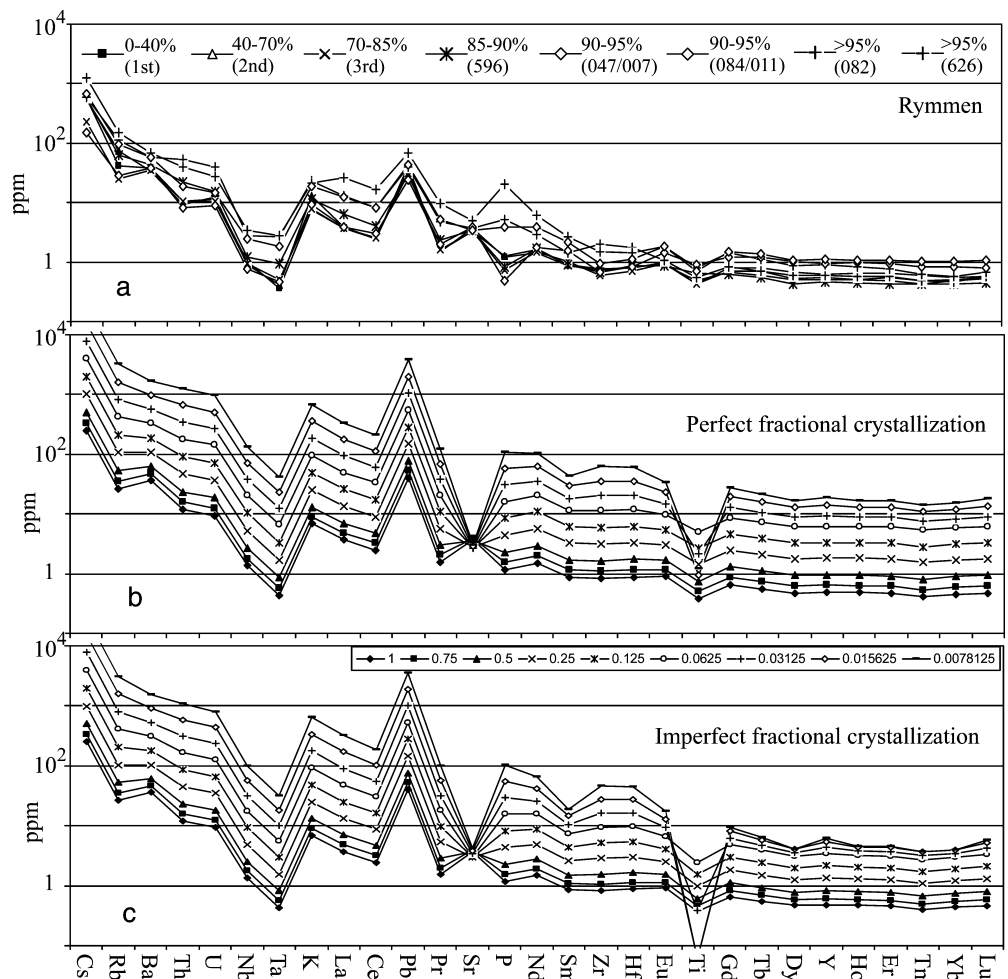
Fig. 11 N-MORB normalized spidergrams showing (**a**) trace-element inversions with estimates of fraction crystallized and model results for perfect (**b**) and imperfect (**c**) fractional crystallization for the Eriksberg gabbro
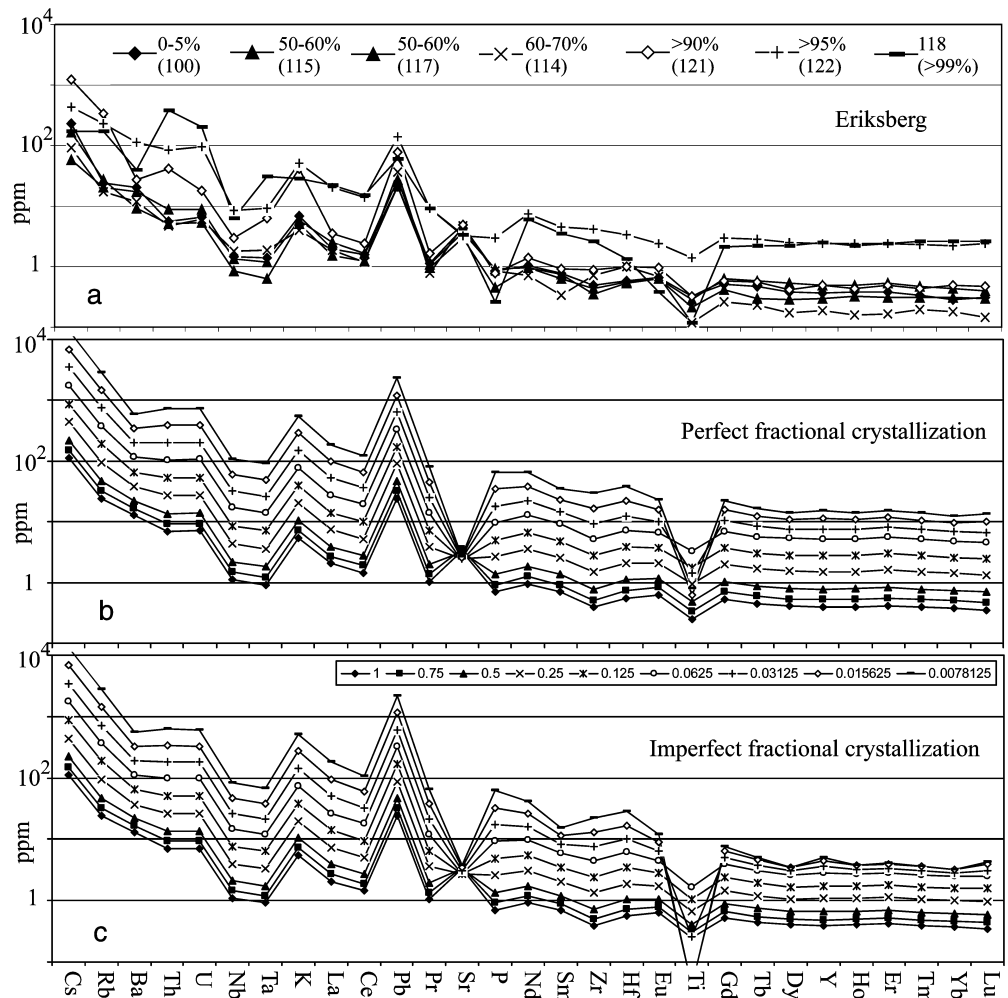
90% crystallized are tightly grouped for the Rymmen gabbro but show a slight range in the Eriksberg gabbro (Figs. 10, 11). The spread in the Eriksberg gabbro may reflect the plotting of individual samples. By averaging three to four inversions of similar rocks from Rymmen gabbro the uncertainty associated with analytical error and estimates of the percent crystallized liquid of the inverted liquid composition is reduced (Bédard 1994). In the Rymmen gabbro, maximum enrichments in the heavy REE are found in the magnetite-bearing rocks with 90 to 95% crystallized while the more incompatible elements are most enriched in samples with >95% crystallized. In the Eriksberg gabbro comparison of a sample with >95% crystallized with a leucotonalite dike, which is taken as a liquid composition, shows them to be very similar with some notable exceptions. Strong depletions in P and Ti in the leucotonalite suggest that both Fe-Ti oxides and apatite were fractionated near the end stages of crystallization (Fig. 11).

Modeled liquid compositions for the Rymmen and Eriksberg gabbros, normalized to normal mid-ocean ridge basalt, show that the parental liquids were enriched in the highly incompatible large-ion lithophile elements but depleted in the moderately incompatible elements, especially the heavy REE (Figs. 10, 11). The patterns from the most primitive troctolites show distinct negative anomalies for Nb, Ta, P, and Ti, minor negative anomalies for Zr and Hf, and positive anomalies for Pb and Sr. The large overall negative slope of the patterns and the anomalies are all consistent with an arc setting for these intrusions (e.g., Tatsumi and Eggins 1995).

Modeling perfect and imperfect fractional crystallization

We modeled the evolution of both intrusions assuming perfect fractional crystallization and imperfect fractionation that includes 10% interstitial amphibole (Figs. 10, 11). The models are based on the following assumptions: (1) After initial infilling, replenishment of the chamber was minimal. This is consistent with the low concentrations of compatible elements in the progressively more evolved rocks suggesting no significant additions of magma occurred. (2) The fraction of the system crystallized can be reasonably estimated from sample locations and compositions as discussed above. (3) The crystallization sequence in the

Eriksberg gabbro is the same as that in the Rymmen gabbro.

Since we can directly observe the fractionating assemblage, the uncertainty involved in using a reconstructed major element composition of the parental liquid, and modeling the fractionation process in terms of major elements to get the mineral proportions, is not required. Rather, the model is based on estimates of the percent crystallized of each type of cumulate in the Rymmen gabbro. Initially this means that olivine and plagioclase are fractionated but as the system evolves clinopyroxene, orthopyroxene, and eventually Fe-Ti oxides and amphibole are included in the cumulus assemblage.

For the imperfect fractional crystallization model we use amphibole as the interstitial phase because it forms as a reaction of the liquid with plagioclase and olivine (Meurer and Claeson 2002) and can be found in even the earliest cumulates. The amphibole is interpreted to have crystallized from interstitial liquid initially in equilibrium with the cumulus assemblage. This crystallization takes place during compaction of the crystal pile and the remainder of the liquid is returned to the supernatant liquid (Meurer and Claeson 2002). This complex process is simplified in the imperfect fractional crystallization model by simply treating amphibole as though it was a

cumulus mineral. The trace-element evolution is then calculated using the same Kd's used in the bulk-rock inversions (Table 4) and other model parameters as summarized in Table 5. We have not included the effects of accessory minerals such as apatite and zircon in these calculations because both the bulk rock P_2O_5 and Zr concentrations and a detailed SEM study of the primitive cumulates reveals that apatite is scarce and zircon absent (work in progress).

Contrasting the perfect and imperfect fractional crystallization models shows that the effect of interstitial amphibole crystallization is most pronounced in the less incompatible elements, especially the heavy REE (Figs. 10, 11). Comparison of the modeled liquid compositions with those of the Rymmen gabbro reveals that even for cumulates thought to represent small fractions of liquid remaining, the trace-element compositions are not nearly as enriched as predicted even by the imperfect crystallization model. The composition of a leucotonalite dike from the Eriksberg gabbro, taken as a liquid, matches the most evolved liquid compositions modeled by imperfect fractional crystallization (Fig. 11). Analysis of liquid compositions from arc settings (Christe and Hannah 1990; Barnes et al. 1990) interpreted to have crystallized from hydrous basaltic liquids reveals that they show trace-element variations similar to those produced by the imperfect fractional crystallization model (Fig. 12).

Table 5 Model parameters used in the trace-element fractionation model

Crystallized (%)	ol	pla	cpx	opx	amp	mag
Perfect fractional crystallization						
25.0	55	45				
50.0	35	65				
75.0	15	65	20			
87.5	10	55	35			
93.8	10	55	25	10		
96.9		45	25	10	15	5
98.4		45	25	10	15	5
99.2		45	25	10	20	
Imperfect fractional crystallization						
25.0	50	40			10	
50.0	30	60			10	
75.0	10	60	20		10	
87.5	10	50	30		10	
93.8	5	50	25	10	10	
96.9		40	20	10	25	5
98.4		40	20	10	25	5
99.2		40	20	10	30	

Conclusions

Characterization of layered gabbroic intrusions crystallized from hydrous basaltic liquids reveals fundamental differences to layered intrusions crystallized from relatively dry basaltic liquids. In primitive gabbroic cumulates formed in dryer intrusions such as the Bushveld and Stillwater complexes, the bulk of whatever crystallized interstitial liquid is present occurs as evolved overgrowths on the cumulus minerals and very little is found as new minerals such as amphibole, apatite, or oxides. In contrast, the high water content of the Rymmen and Eriksberg gabbros helped to stabilize amphibole early during the cooling of the crystal mush at the floor of the intrusions. The reaction of liquid with plagioclase and olivine (Meurer and Claeson 2002) allowed a significant amount of amphibole to crystallize

Fig. 12 Comparison of basaltic liquids from arc settings from the literature shown as *grey fields* (data from Christe and Hannah 1990; Barnes et al. 1990) and the calculated most primitive liquids of this study in a N-MORB normalized spidergram
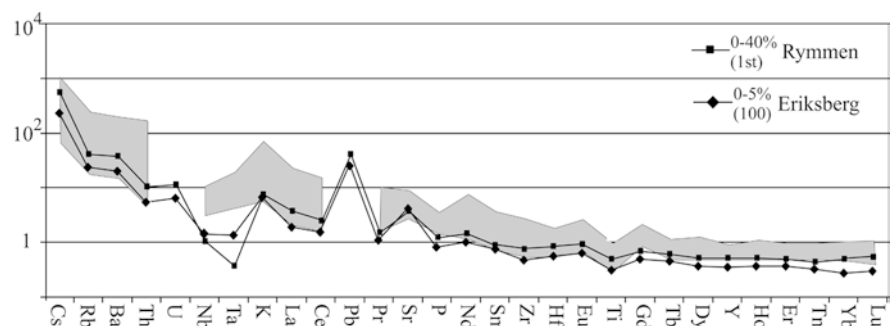
over a small temperature range. Thus compaction, diffusion, and/or other postcumulus processes that can reduce the fraction of interstitial liquid in dryer intrusions, did not operate efficiently. The incorporation of a large proportion of amphibole strongly modified the bulk D of the interstitial assemblage. The return of liquid from the crystal pile after amphibole saturation is reflected in the relative depletions of elements more compatible in amphibole (e.g., the middle REE, Ti, V, etc.) while elements that are very incompatible in amphibole are enriched. The result of these relative depletions and enrichments is to steepen the MORB normalized trace-element patterns with progressive fractionation.

Recent arc-cumulates are studied by the mineral assemblages and compositions of ejected plutonic blocks from arc volcanic associations (e.g., Arculus and Wills 1980; Conrad and Kay 1984; Beard and Borgia 1989; Pearce et al. 1995; Morra et al. 1997; Warner and Wasilewski 1997). The lack of stratigraphic control on these samples makes it problematic to understand how the separation of liquid from crystals and the crystallization of interstitial liquid contribute to the evolution of these liquids. The growth of amphibole as an interstitial phase may be responsible for both its apparent involvement in the fractionation of basaltic liquids in arc settings, and the paucity of amphibole phenocrysts in the erupted basaltic liquids (e.g., Bédard et al. 1987; Romick et al. 1992; Kay and Kay 1985). For example, consider a volcano tapping either the Rymmen or Eriksberg magma chambers after 20% crystallization and the return of some evolved liquid from the crystal pile. The lava generated would be basaltic (based on the fractionating assemblage), would not be saturated in amphibole, but would have some trace-element characteristics of amphibole fractionation because of the returned liquid from the crystal pile. Short of dismembering the cumulus pile, the interstitial amphibole will not be found in the erupted basaltic liquids because it is not a liquidus phase *in the magma chamber*. Thus, although amphibole is unavailable for inclusion as a phenocryst it still imparts a chemical signature to the lava compositions. The concept and mechanism of imperfect fractional crystallization developed here has many similarities with the in situ fractionation model proposed by Langmuir (1989) and has general importance for the study of volcanic rocks and the reliance on phenocryst assemblages to infer how fractionation might have modified liquid compositions.

References

Anderson AT Jr (1980) Significance of hornblende in calc-alkaline andesites and basalts. Am Mineral 65:837–851

Arculus RJ, Wills KJA (1980) The petrology of plutonic blocks and inclusions from the Lesser Antilles Island Arc. J Petrol 21:743–799

Ariskin AA, Barmina GS (1999) An empirical model for the calculation of spinel-melt equilibria in mafic igneous systems at atmospheric pressure: 2. Fe-Ti oxides. Contrib Mineral Petrol 134:251–263

Barnes CG, Allen CM, Hoover JD, Brigham RH (1990) Magmatic components of a tilted plutonic system, Klamath Mountains, California. In: Anderson JL (ed) The nature and origin of Cordilleran magmatism. Geol Soc Am Mem 174, pp 331–346

Bartels KS, Kinzler RJ, Grove TL (1991) High-pressure phase relations of primitive high-alumina basalts from Medicine Lake volcano, northern California. Contrib Mineral Petrol 108:253–270

Beard JS, Borgia A (1989) Temporal variation of mineralogy and petrology in cognate gabbroic enclaves at Arenal volcano, Costa Rica. Contrib Mineral Petrol 103:110–122

Beard JS, Lofgren GE (1992) An experiment-based model for the petrogenesis of high-alumina basalts. Science 258:112–115

Beattie P (1993) Olivine-melt and orthopyroxene-melt equilibria. Contrib Mineral Petrol 115:103–111

Bédard JH (1994) A procedure for calculating the equilibrium distribution of trace elements among the minerals of cumulate rocks, and the concentration of trace elements in the coexisting liquids. Chem Geol 118:143–153

Bédard JH (2001) Parental magmas of the Nain Plutonic Suite anorthosites and mafic cumulates: a trace element modeling approach. Contrib Mineral Petrol 141:747–771

Bédard JH, Ludden J, Francis D (1987) The Mégantic intrusive complex of Québec: a study of the derivation of silica oversaturated anorogenic magmas of alkaline affinity. J Petrol 28:355–388

Bindeman IN, Bailey JC (1999) Trace elements in anorthite megacrysts from the Kurile Island Arc: a window to across-arc geochemical variations in magma compositions. Earth Planet Sci Lett 169:209–226

Blundy J (1997) Experimental study of a Kiglapait marginal rock and implications for trace element partitioning in layered intrusions. Chem Geol 141:73–92

Blundy JD, Shimizu N (1991) Trace element evidence for plagioclase recycling in calc-alkaline magmas. Earth Planet Sci Lett 102:178–197

Burnham WC (1979) The importance of volatile constituents. In: Yoder HS Jr (ed) The evolution of the igneous rocks: Fiftieth anniversary perspectives. Princeton University Press, Princeton, New Jersey, pp 439–482

Canil D, Fedortchouk Y (2001) Olivine-liquid partitioning of vanadium and other trace elements, with applications to modern and ancient picrites. Can Mineral 39:319–330

Cawthorn RG (1994) Formation of chlor- and fluor-apatite in layered intrusions. Mineral Mag 58:299–306

Cawthorn RG (ed) (1996) Layered intrusions. Elsevier, Amsterdam

Chazot G, Menzies MA, Harte B (1996) Determination of partition coefficients between apatite, clinopyroxene, amphibole, and melt in natural spinel lherzolites from Yemen: implications for wet melting of the lithospheric mantle. Geochim Cosmochim Acta 60:423–437

Christe G, Hannah JL (1990) High-K, continental-arc volcanism in the Kettle Rock sequence of the eastern Mesozoic belt, northern Sierra Nevada, California: implications for lower Mesozoic Cordilleran tectonics. In: Anderson JL (ed) The nature and origin of Cordilleran magmatism. Geol Soc Am Mem 174, pp 315–329

Claeson DT (1998) Coronas, reaction rims, symplectites and emplacement depth of the Rymmen gabbro, Transscandinavian Igneous Belt, southern Sweden. Mineral Mag 62:743–757

Claeson DT (1999a) Corundum-bearing ultramafic veins in the Rymmen gabbro, southern Sweden: isochemical mineral alteration. Neues Jahrb Mineral Abh 175:1–27

Claeson DT (1999b) Geochronology of the Rymmen gabbro, southern Sweden; implications for primary versus inherited zircon in mafic rocks and rheomorphic dykes. GFF 121: 25–31

Claeson DT (2001) Investigation of gabbroic rocks associated with the Småland-Värmland granitoid batholith of the Transscandinavian Igneous Belt, Sweden. Doctoral Thesis A64, Earth Sciences Centre, Göteborg University

Claeson DT (2002) Stability of REE-bearing minerals in a metaluminous leucotonalite from the Eriksberg gabbro, Transscandinavian Igneous Belt, Sweden. Neues Jahrb Mineral Abh 177:277–291

Claeson DT, Meurer WP (2002) An occurrence of igneous orthorhombic amphibole, Eriksberg gabbro, southern Sweden. Am Mineral 87:699–708

Conrad WK, Kay RW (1984) Ultramafic and mafic inclusions from Adak Island: crystallization history, and implications for the nature of primary magmas and crustal evolution in the Aleutian Arc. J Petrol 25:88–125

Dunn T (1987) Partitioning of Hf, Lu, Ti, and Mn between olivine, clinopyroxene and basaltic liquid. Contrib Mineral Petrol 96:476–484

Dunn T, Sen C (1994) Mineral/matrix partition coefficients for orthopyroxene, plagioclase, and olivine in basaltic to andesitic systems: a combined analytical and experimental study. Geochim Cosmochim Acta 58:717–733

Frost BR, Lindsley DH, Andersen DJ (1988) Fe-Ti oxide-silicate equilibria: assemblages with fayalitic olivine. Am Mineral 73:727–740

Gaál G, Gorbatschev R (1987) An outline of the Precambrian evolution of the Baltic Shield. Precambrian Res 35:15–52

Gaetani GA, Grove TL, Bryan WB (1993) The influence of water on the petrogenesis of subduction-related igneous rocks. Nature 365:332–334

Ghiorso MS, Carmichael ISE (1985) Chemical mass transfer in magmatic processes II. Applications in equilibrium crystallisation, fractionation and assimilation. Contrib Mineral Petrol 90:121–141

Ghiorso MS, Carmichael ISE (1987) Modeling magmatic systems: petrologic applications. In: Carmichael ISE, Eugster HP (eds) Thermodynamic modeling of geological materials: minerals, fluids and melts. Mineral Soc Am Rev Mineral 17:467–499

Gorbatschev R (1980) The Precambrian development of southern Sweden. Geologiska Föreningens i Stockholm Förhandlingar 102:129–136

Grove TL, Parman SW, Bowring SA, Price RC, Baker MB (2002) The role of an H$_2$O-rich fluid component in the generation of primitive basaltic andesites and andesites from the Mt. Shasta region, N California. Contrib Mineral Petrol 142:375–396

Hammarstrom JM, Zen E (1986) Aluminium in hornblende: an empirical igneous geobarometer. Am Mineral 71:1297–1313

Holland T, Blundy J (1994) Non-ideal interactions in calcic amphiboles and their bearing on amphibole-plagioclase thermometry. Contrib Mineral Petrol 116:433–447

Imai N, Terashima S, Itoh S, Ando A (1995) 1994 compilation of analytical data for minor and trace elements in seventeen GSJ geochemical reference samples, "Igneous Rock Series". Geostand Newsl 19:135–213

Johnson MC, Rutherford MJ (1989) Experimental calibration of the aluminium-in-hornblende geobarometer with application to Long Valley caldera (California) volcanic rocks. Geology 17:837–841

Juhlin C, Wahlgren C-H, Stephens MB (2000) Seismic imaging in the frontal part of the Sveconorwegian orogen, south-western Sweden. Precambrian Res 102:135–154

Kay SM, Kay RW (1985) Aleutian tholeiite and calc-alkaline magmas series I: the mafic phenocrysts. Contrib Mineral Petrol 90:276–290

Kennedy AK, Lofgren GE, Wasserburg GJ (1993) An experimental study of trace element partitioning between olivine, orthopyroxene and melt in chondrules: equilibrium values and kinetic effects. Earth Planet Sci Lett 115:177–195

Kinzler RJ, Donnelly-Nolan JM, Grove TL (2000) Late Holocene hydrous mafic magmatism at the Paint Pot Crater and Callahan flows, Medicine Lake Volcano, N California and the influence of H$_2$O in the generation of silicic magmas. Contrib Mineral Petrol 138:1–16

Kohn SC, Schofield PF (1994) The importance of melt composition in controlling trace-element behaviour: an experimental study of Mn and Zn partitioning between forsterite and silicate melts. Chem Geol 117:73–87

Kuritani T (1998) Boundary layer crystallization in a basaltic magma chamber: evidence from Rishiri Volcano, northern Japan. J Petrol 39:1619–1640

Kushiro I (1979) Fractional crystallization of basaltic magma. In: Yoder HS Jr (ed) The evolution of the igneous rocks: fiftieth anniversary perspectives. Princeton University Press, Princeton, NJ, pp 171–203

Langmuir CH (1989) Geochemical consequences of the solidification of magma chambers through "in situ" crystallization. Nature 340:199–205

Larson SÅ, Berglund J, Stigh J, Tullborg E-L (1990) The Protogine Zone, southwest Sweden: a new model—an old issue. In: Gower CF, Rivers T, Ryan B (eds) Mid-Proterozoic Laurentia. Baltica. Geol Assoc Can Spec Pap 38, pp 317–333

Longhi J, Vander Auwera J, Fram MS, Duchesne J-C (1999) Some phase equilibrium constraints on the origin of Proterozoic (Massif) anorthosites and related rocks. J Petrol 40:339–362

Lundegårdh PH (1987) Description to the map of solid rocks Filipstad SW. SGU Series Af 157

Lundstrom CC, Shaw HF, Ryerson FJ, Williams Q, Gill J (1998) Crystal chemical control of clinopyroxene-melt partitioning in the Di-Ab-An system: implications for elemental fractionations in the depleted mantle. Geochim Cosmochim Acta 62:2849–2862

Magnusson NH (1925) Persbergs malmtrakt och berggrunden i de centrala delarna av Filipstads bergslag i Värmlands län. Kungl. Kommerskollegium, Beskrivningar över mineralfyndigheter, Nr 2.

Meurer WP, Boudreau AE (1996) Compaction of density stratified cumulates: effect on trapped-liquid distributions. J Geol 104:115–120

Meurer WP, Boudreau AE (1998a) Compaction of igneous cumulates, Part I: geochemical consequences for cumulates and liquid fractionation trends. J Geol 106:281–292

Meurer WP, Boudreau AE (1998b) Compaction of igneous cumulates, Part II: compaction and the development of igneous foliations. J Geol 106:293–304

Meurer WP, Claeson DT (2002) Evolution of crystallizing interstitial liquid in an arc-related cumulate determined by LA ICP-MS mapping of a large amphibole oikocryst. J Petrol 43:607–629

Morra V, Secchi FAG, Melluso L, Franciosi L (1997) High-Mg subduction-related Tertiary basalts in Sardinia, Italy. Lithos 40:69–91

Müntener O, Kelemen PB, Grove TL (2001) The role of H$_2$O during crystallization of primitive arc magmas under uppermost mantle conditions and genesis of igneous pyroxenites: an experimental study. Contrib Mineral Petrol 141:643–658

Nielsen RL, Gallahan WE, Newberger F (1992) Experimentally determined mineral-melt partition coefficients for Sc, Y and REE for olivine, orthopyroxene, pigeonite, magnetite and ilmenite. Contrib Mineral Petrol 110:488–499

Panjasawatwong Y, Danyushevsky LV, Crawford AJ, Harris KL (1995) An experimental study of the effects of melt composition on plagioclase—melt equilibria at 5 and 10 kbar: implications for the origin of magmatic high-An plagioclase. Contrib Mineral Petrol 118:420–432

Parsons I (ed) (1987) Origins of igneous layering. D Reidel, Dordrecht

Pearce JA, Baker PE, Harvey PK, Luff IW (1995) Geochemical evidence for subduction fluxes, mantle melting and fractional crystallization beneath the south Sandwich Island Arc. J Petrol 36:1073–1109

Philpotts AR, Maureen C, Hill JM (1996) Crystal-mush compaction and the origin of pegmatitic segregation sheets in a thick flood-basalt flow in the Mesozoic Hartford Basin, Connecticut. J Petrol 37:811–836

Philpotts JA, Schnetzler CC (1970) Phenocryst-matrix partition coefficients for K, Rb, Sr and Ba, with applications to anorthosite and basalt genesis. Geochim Cosmochim Acta 34:307–322

Roeder PL, Emslie RF (1970) Olivine-liquid equilibrium. Contrib Mineral Petrol 29:275–289

Powell R (1978) The thermodynamics of pyroxene geotherms. Philos Trans R Soc Lond A 288:457–469

Rollinson H (1993) Using geochemical data: evaluation, presentation, interpretation. Longman Group UK, Harlow

Romick JD, Kay SM, Kay RW (1992) The influence of amphibole fractionation on the evolution of calc-alkaline andesite and dacite tephera from the central Aleutians, Alaska. Contrib Mineral Petrol 112:101–118

Shi P (1993) Low-pressure phase relationships in the system Na_2O-CaO-FeO-MgO-Al_2O_3-SiO_2 at 1,100 °C, with implications for the differentiation of basaltic magmas. J Petrol 34:743–762

Shirley DN (1986) Compaction of igneous cumulates. J Geol 94:795–809

Shirley DN (1987) Differentiation and compaction in the Palisades sill, New Jersey. J Petrol 28:835–865

Sisson TW, Grove TL (1993a) Experimental investigations of the role of H_2O in calc-alkaline differentiation and subduction zone magmatism. Contrib Mineral Petrol 113:143–166

Sisson TW, Grove TL (1993b) Temperatures and H_2O contents of low-MgO high-alumina basalts. Contrib Mineral Petrol 113:167–184

Snyder D, Carmichael ISE, Wiebe RA (1993) Experimental study of liquid evolution in an Fe-rich, layered mafic intrusion: constraints of Fe-Ti oxide precipitation on the T-fO_2 and T-r paths of tholeiitic magmas. Contrib Mineral Petrol 113:73–86

Sun SS, McDonough WF (1989) Chemical and isotopic systematics of oceanic basalts: implications for mantle composition and processes. In: Saunders AD, Norry MJ (eds) Magmatism in ocean basins. Geol Soc Lond Spec Publ 42, pp 313–345

Tatsumi Y, Eggins S (1995) Subduction zone magmatism. Blackwell Scientific Publications, Oxford

Toplis MJ, Carroll MR (1995) An experimental study of the influence of oxygen fugacity on Fe-Ti oxide stability, phase relations, and mineral-melt equilibria in ferro-basaltic systems. J Petrol 36:1137–1170

Vinnefors A (1985) Post-Svecokarelian basic plutonics and bronzite diabases in eastern Värmland, Sweden. Diss Geol Inst A 50, Göteborg

Vogel DC, Keays RR, James RS, Reeves SJ (1999) The geochemistry and petrogenesis of the Agnew intrusion, Canada: a product of S-undersaturated, high-Al and low-Ti tholeiitic magmas. J Petrol 40:423–450

Wahlgren CH, Cruden AR, Stephens MB (1994) Kinematics of a major fan-like structure in the eastern part of the Sveconorwegian orogen, Baltic Shield, south-central Sweden. Precambrian Res 70:67–91

Warner RD, Wasilewski PJ (1997) Magnetic petrology of arc xenoliths from Japan and Aleutian Islands. J Geophys Res 102:20225–20243

Watson EB, Ben Othman D, Luck J-M, Hofmann AW (1987) Partitioning of U, Pb, Cs, Yb, Hf, Re and Os between chromian diopsidic pyroxene and haplobasaltic liquid. Chem Geol 62:191–208

Wells PRA (1977) Pyroxene thermometry in simple and complex systems. Contrib Mineral Petrol 62:129–139

Wikman H (2000) Description to the maps of solid rocks 5E Växjö NE and NW. SGU Series Af 201 and 216

Wood BJ, Banno S (1973) Garnet-orthopyroxene and orthopyroxene-clinopyroxene relationships in simple and complex systems. Contrib Mineral Petrol 42:109–124

Wood BJ, Blundy JD (1997) A predictive model for rare earth element partitioning between clinopyroxene and anhydrous silicate melt. Contrib Mineral Petrol 129:166–181